Topics in Catalysis (2019) 62:786–794
https://doi.org/10.1007/s11244-019-01180-3

ORIGINAL PAPER

Effect of the Nature of Metal Nanoparticles on the Photocatalytic Degradation of Rhodamine B

Ahmad S. Alshammari[1] · Abdulaziz Bagabas[1] · Naif Alarifi[1] · Rashid Altamimi[1]

Published online: 29 June 2019
© Springer Science+Business Media, LLC, part of Springer Nature 2019

Abstract
Rhodamine B (RhB), which has several industrial and chemical applications, is a harmful dye. It requires treatment prior to discharging for both environmental and societal safety. In this context, titania (denoted as DTS) supported different types of noble metal nanoparticles, with one percent weight per weight loading of metal. These were synthesized and were applied for RhB photodegradation. The synthesized photocatalysts were characterized by BET surface area, X-ray powder diffraction (XRPD), transmission electron microscopy (TEM), solid-state UV–Vis, H_2-TPR study, CO-pulse chemisorption analysis. The activity of 1% noble metals/DTS for RhB photodegradation under UV irradiation follows the order of Pt/DTS > Pd/DTS > Ru/DTS > DTS. The most optimal activity of Pt/DTS could be attributed to its lowest reflectance and highest degree of absorbance of UV light, its smallest band gap energy (E_g) and its moderate interactions with DTS support.

Keywords Photocatalyst · Metal nanoparticles · Rhodamine B · Titanium dioxide · Organic dyes

1 Introduction

Many types of organic dyes are released into the global environment on a yearly basis. This effluent is released via wastewaters generated from a number of industries [1–3]. Organic dyes which are produced on a large scale, such as RhB, are of the most concerning examples due to their toxicity in relation to the environment and their slow rates of both biodegradation and decolouration [4]. Various established methods have been investigated and applied to eliminate these pollutants e.g. [5, 6]. The process of photocatalytic degradation is one of the most renowned removal methods for organic dyes. This process works by irradiating a semiconductor metal oxide photocatalyst with suitable light wavelengths [7–10]. This method of removing the pollutants from wastewater has recently been investigated extensively as an emerging renewable technology, using TiO_2.

TiO_2, one of the most applied metal oxide photocatalysts, is popular due to a number of features. These include the following: nontoxicity, photo-stability, high oxidative power and reusability, amongst other properties [11–17]. However, it has numerous drawbacks which lower its photocatalytic activity including: poor light utilization, low adsorption ability, agglomeration, difficulty in separation and the ease by which photocatalytic activity is lost [18]. In addition, the photocatalytic activity of TiO_2 is restricted by its wide E_g, where narrowing its E_g. This would not only act as a sensitizer, but also reduce the recombination rate of the photogenerated electron–hole pairs, this giving rise to an enhancement of its photocatalytic activity. These drawbacks can be overcome, for instance, by loading different noble metal nanoparticles such as ruthenium (Ru), palladium (Pd), or platinum (Pt) over DTS [19–22]. The enhancement of photocatalytic activity by the loading of noble metal nanoparticles is not limited to the capturing of electrons by the Schottky barriers [23, 24]. However, noble metal nanoparticles are usually employed in order to minimize the band gap energy and recombination rate [25].

The photocatalytic activity of supported noble metal nanoparticles (e.g. Pd, Au, Pt, etc.) is usually controlled by various factors including: particle size, phase structure, BET surface area and metal-support interactions [26–29]. This is due to the fact that such factors would control the

✉ Ahmad S. Alshammari
aalshammari@kacst.edu.sa

✉ Abdulaziz Bagabas
abagbas@kacst.edu.sa

[1] Materials Science Research Institute, King Abdulaziz City for Science and Technology, P.O. Box 6086, Riyadh 1442, Kingdom of Saudi Arabia

amount of adsorbed organic molecules on the surface of the catalyst, which in turn enhance the degradation rate. All of these factors can be controlled by immobilizing noble metal nanoparticles over the surface and within the pores of TiO_2 support. The majority of investigations on noble metal photocatalytic degradation of RbB were obtained using TiO_2 (Degussa P25) [30–32]. These were typically performed with the anatase shape having a specific BET-surface area of 50 m^2/g corresponding to an average particle size ranging between 20 and 30 nm [33, 34]. However, limited studies related to the effect of the nature of TiO_2 on the photocatalytic degradation of RhB under UV light have been reported. For instance, Ohno et al. and others [35, 36] reported that a mixture of anatase and rutile phases was found to be a more active catalyst compared to pure anatase due to semiconductor/semiconductor heterojunction. In addition, it was reported that TiO_2-P25 degraded the dye much more rapidly compared to other photocatalysts [37, 38]. Giwa et al. [39] compared the degradation performance of TiO_2-P25 and TiO_2 and found TiO_2-P25 to be more active for photodegradation. The best photoreactivity of TiO_2-P25 is due to the slow recombination of the electron–hole pair and its large surface area [40]. Most of the published work showed that the efficiency of photocatalysts depends on different factor such as the light source and its intensity, pH value, the amount of the photocatalyst, the concentration of the dye, the irradiation time, etc. Therefore, it will be hard to compare the photoactivity of our photocatalysts with those previously published in the literature.

As the photocatalytic efficiency of TiO_2 was reported to be influenced by several features, such as particle size [41, 42] crystalline structure [43, 44], doping with the other metal [45, 46], or reduced and defect TiO_2 engineering [47], the present study, therefore, aims to explore the photodegradation of RhB by using rarely used TiO_2 materials (DTS, Cristal Corporate). We also propose an alternative and simple approach to synthesize our photocatalysts by reducing the Ru, Pd, and Pt acetylacetonate complexes, loaded on the DTS surface via the wet impregnation method. The ultimately synthesized photocatalysts were characterized by inductively-coupled plasma optical emission spectroscopy (ICP-OES), N_2-physisorption, solid-state UV–Vis absorbance and reflectance spectrophotometry, X-ray powder diffraction (XPRD), and transmission electron microscopy (TEM). The photocatalytic degradation of RhB in an aqueous medium over these photocatalysts enabled disclosures regarding the effect of metal NPs nature on the photocatalytic activity.

2 Materials and Methods

2.1 Materials

Ruthenium(III), palladium(II), and platinum(II) acetylacetonate complexes (Aldrich), titanium dioxide (DTS, Cristal Corporate), methanol (Sigma-Aldrich), rhodamine B (≥ 95% HPLC, Sigma) were commercially accessible and were used as received. Deionized water (18.2 MΩ cm) was supplied by using the Milli-Q water purification system (Millipore).

2.2 Catalyst Synthesis

Spherical Ru, Pd and Pt NPs supported on commercial DTS titanium dioxide were obtained in two-step synthesis procedure by using wet impregnation method. In the first step, a specific amount of acetone solution of noble metal acetylacetonate was impregnated to a certain amount of DTS. The resultant mixtures were ultrasonicated at room temperature for an hour by using an ultrasonic bath to disperse the DTS support. In the second step, after solvent evaporation, the obtained solid samples were oven-dried at 80 °C for 2 h, followed by H_2 reduction at 150 °C for 2 h to come up with 1.0 wt/wt% noble metal nanoparticles (Ru, Pd, and Pt) supported on DTS.

2.3 Characterization

Nobel metal content in each photocatalyst was determined by using a Varian Vista-MPX ICP-OES instrument. The specific surface area, based on the Brunauer–Emmett–Teller method (S_{BET}) was assessed by N_2 physisorption at − 196 °C by using a Micromeritics ASAP 2010 adsorption analyzer. XRPD patterns were obtained by using a D8 advance Bruker instrument. This operated at 40 mA and 40 kV using CuK_α radiation and a Ni filter in the 2-theta range between 10° and 80°. To observe the morphology and particle sizes of the photocatalysts, a JEM-2100F JEOL TEM was used. Solid-state UV–Vis absorbance and reflectance spectra for photocatalysts were recorded by using a PerkinElmer Lambda 950 UV/Vis/NIR spectrophotometer. The XPS analyses were carried out on a PHI 5000 VersaProbe-Scanning ESCA microprobe (ULVAC-PHI, Japan/USA) instrument at a base pressure of 5.5×10^{-7} Pa, where the X-ray source of Al-K_α ($h\nu = 1486.6$ eV) with a spot size of 200 µm was used. Temperature programmed reduction (TPR) and CO-pulse chemisorption studies were conducted using a Micromeritics AutoChem II 2920. Reduction profiles were achieved by passing a mixture of 10% H_2/Ar (TPR) and 10% CO/Ar (CO-pulse chemisorption) at a rate of 50 mL/min (STP) over 0.1 g of photocatalyst. The temperature was gradually increased from room temperature to 500 °C at a heating rate

Table 1 Metal content (%), S_{BET} and V_p results of noble metals supported on DTS

Catalysts	Metal content (wt%)	S_{BET} (m^2/g)	V_p (cm^3/g)	Noble metal particle size (nm)	E_g
DTS	–	107.5	0.335	–	3.06
Pd/DTS	1.08	100.6	0.301	3–6	2.90
Ru/DTS	0.95	102.4	0.332	3–5	2.75
Pt/DTS	0.93	102.7	0.334	1–3	2.70

of 10 °C/min. The total consumption of H_2 was calculated by a thermal conductivity detector (TCD) as a function of temperature.

2.4 Photocatalytic Test

The photocatalytic tests were executed by using 100 mg of photocatalyst in a beaker containing 100 mL, 20 mg/L of RhB. Tests were conducted using a Luzchem Photoreactor (model CCP-4 V; top and side irradiation; Luzchem Research Incorporation, Canada) at room temperature, under ambient air without bubbling. Prior to exposing the reaction mixture to UV irradiation, the reaction mixture was stirred magnetically (300 rpm) in the dark for an hour to attain the adsorption/desorption equilibrium of the dye on the surface of the photocatalyst. Subsequently, the reaction suspension was exposed to UV-A light radiation, with a wavelength maximum of 365 nm, at a power of 54.3 W/m^2. At an interval of 10 min, a 5.0 mL sample was drawn by syringe from the irradiated reaction mixture and was centrifuged for 30 min to separate the photocatalyst from the mixture. Using a UV/Vis/NIR spectrophotometer, the typical absorbance of RhB at 554 nm was selected to calculate the equilibrium concentrations of RhB at various reaction times, where the equilibrium concentration was inversely linked with the degradation percentage of RhB.

3 Results and Discussion

3.1 Chemical Composition and N_2-Physisorption

Table 1 summarizes the chemical and textural analysis results for the photocatalysts. ICP analysis. This provided precise results which corresponded with the nominal content of noble metal (i.e. 1 wt% of Ru, Pd, or Pt). N_2-physisorption was executed to assess the Brunauer–Emmett–Teller specific surface area (S_{BET}) and the total pore volume (V_p). These were found to marginally decreased with the changing the nature of the supported noble metal. Such results are in line with the partial filling of the titanium dioxide pores by the noble metal nanoparticles.

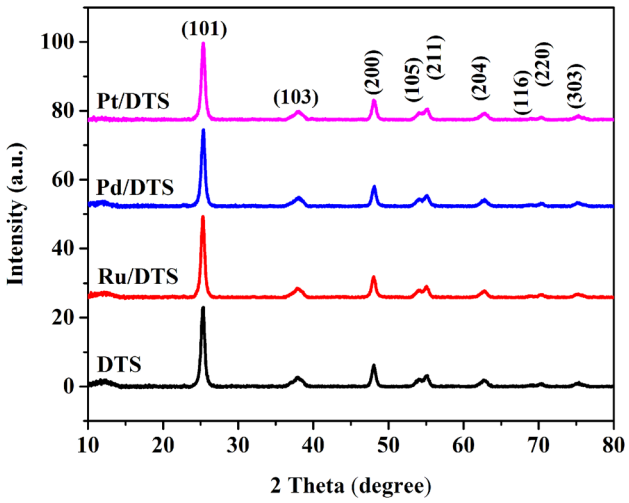

Fig. 1 XRD patterns of Pd, Ru and Pt metal nanoparticles supported on DTS photocatalysts

3.2 XRD Phase Identification

The crystalline phase and crystallinity of the prepared photocatalysts were identified by using XRD. Figure 1 illustrates the diffraction patterns of Ru, Pd and Pt supported on DTS photocatalysts, where peaks related to DTS were detected, as confirmed by the presence of diffraction peaks at 2θ values of 25.4°, 37.9°, 48.1°, 54.0°, and 55.2°, which correspond to (101), (004), (200), (105) and (211) crystallographic planes of anatase, respectively. In addition, Fig. 1 discloses no diffraction patterns related to metallic Ru, Pd and Pt. This result is in accordance with TEM results as the metal NPs were well dispersed with small particles (≤ 5 nm).

3.3 TEM Microscopy Analysis

The morphology and size determination of different metal NPs supported on DTS were obtained through using the TEM technique. Figure 2 shows that all of the prepared three photocatalysts have spherical metal nanoparticles. PtNPs supported on DTS showed somewhat smaller, uniform particle size with a narrow average size of 2 nm in comparison to the particle size of Pd and Ru, supported on DTS, ranging between 1 and 5 nm. Furthermore, HRTEM revealed that Pt, Pd and Ru metal nanoparticles, supported on DTS, were crystalline. The lattice plane fringes of the different noble metal nanoparticles were used to estimate the value of d-spacing and were compared with those which corresponding corresponded to the bulk of each metal. These values were found to correspond to Ru (111), Pd (111) and Pt (110) crystal planes, respectively.

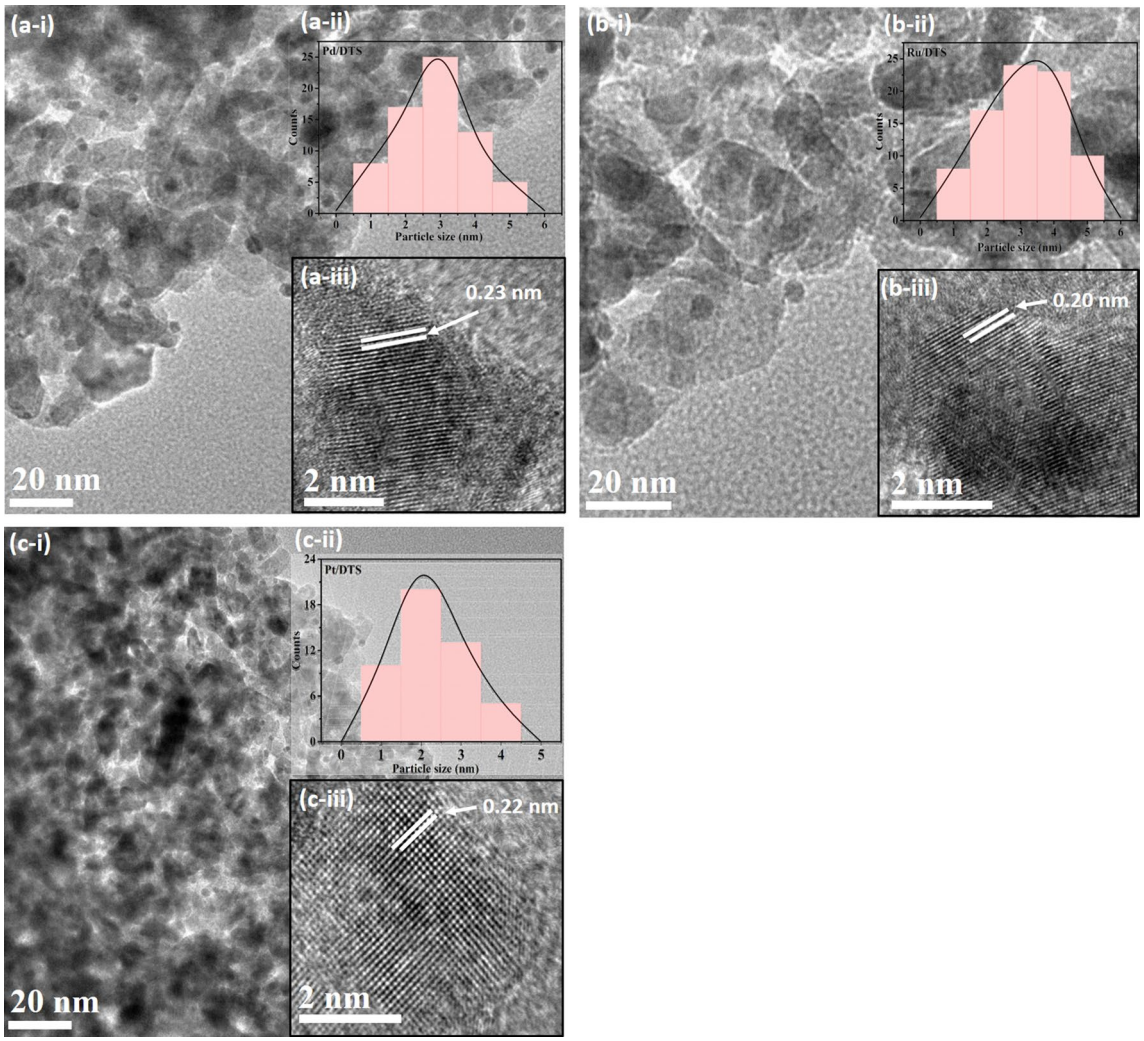

Fig. 2 TEM images of Pd (**a-i**), Ru (**b-i**), and Pt (**c-i**) NPs supported on DTS. The inset histogram of particle size distribution of Pd (**a-ii**), Ru (**b-ii**), and Pt (**c-ii**) NPs supported on DTS. The inset HRTEM images of observed crystal planes of Pd (**a-iii**), Ru (**b-iii**), and Pt (**c-iii**) NPs supported on DTS

3.4 Solid-State UV–Vis Spectrophotometry

Figure 3 displays the UV–Vis absorbance (A) and reflectance (B) spectra of pure DTS and the 1.0 wt/wt% noble metal nanoparticles supported on DTS (note that the SPR of Ru, Pd and Pt NPs are observed in the middle UV, i.e. between 175 and 200 nm). Pure DTS displayed absorbance from 200 to 390 nm with marginal absorbance in the visible region. However, upon loading the noble metal nanoparticles on DTS, both the absorbance in the UV and visible regions were enhanced, where Pt resulted in the highest absorbance, followed by Ru and finally by Pd. In parallel to this observation, as anticipated, Pt/DTS showed the minimum degree of reflectance of both UV and visible light, while higher reflectance for this light was observed by Ru/DTS and much higher reflectance by Pd/DTS. DTS showed the highest degree of reflectance.

The indirect E_g of the pure DTS and the Pd, Ru and Pt NPs supported on DTS are presented in Fig. 3c, where the x-axis represents the photon energy E in eV and y-axis is the square root of the product of the absorption coefficient (α) and energy $(E\alpha)^{0.5}$. The estimated E_g of pure DTS was 3.06 eV, while it reduced after Pd, Ru, and Pt loading to 2.90, 2.75, and 2.70 eV, respectively. These changes indicated that the optical properties of the photocatalyst were affected by the nature of the noble metal applied. The reduction in the band gap of DTS after loading noble metal nanoparticles could be attributed to their interaction with the DTS support because DTS is well-known for exhibiting such behavior [48, 49]. This conclusion was supported by TPR study (vide infra). The highest absorbance, lowest reflectance and smallest E_g of Pt/DTS are key

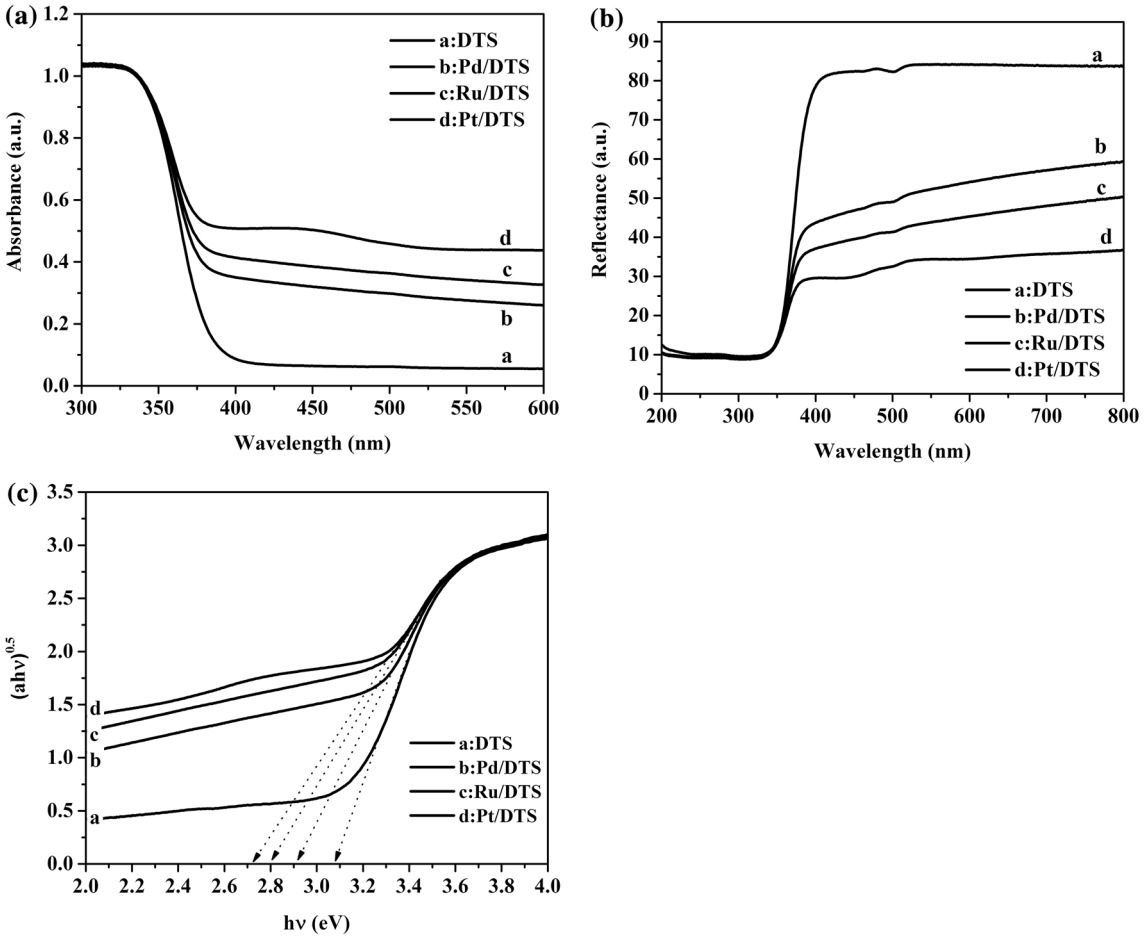

Fig. 3 UV–Vis absorbance (**a**), reflectance (**b**) spectra, indirect E_g (**c**) of pure DTS and the 1.0 wt/wt% noble metal nanoparticles supported on DTS

factors for expecting its superiority as a photocatalyst over the tested photocatalysts with inferior optical characteristics. This expectation was confirmed by the observed photocatalytic activity which was discussed later.

3.5 Temperature Programmed Reduction (TPR) Analysis

TPR is an important tool for qualitatively studying the strong-metal-support-interaction (SMSI) phenomenon and evaluating the reducibility of the catalysts. Figure 4 displays the hydrogen temperature programmed reduction (H_2-TPR) profiles obtained for pure DTS and for 1wt/wt% Pd, Ru, or Pt supported on DTS catalysts. TPR of Pure DTS showed a broad peak between 250 and 400 °C, ascribed probably to the reduction of TiO_2 to some TiO_x or Ti_yO_x. On the other hand, all noble metal nanoparticles which supported photocatalyst samples revealed two reduction peaks ranging between 50 and 180 °C, where the positions of these peaks depended on the type of noble metal nanoparticles. The first peak could be ascribed to the reduction of the noble metal, while the second peak could be ascribed to the noble metal nanoparticle interaction with the DTS support. The first peak in the TPR profile of Ru was sharp, well-resolved from the second peak and ended at ~ 75 °C. However, the first peak in the TPR profile of Pd was somewhat sharp with a maximum of ~ 75 °C and overlapped with the second peak.

Furthermore, the first peak in the TPR profile of Pt was broad with a shoulder. It began at ~ 100 °C, ended at ~ 150 °C and then overlapped with the second peak. The second peak in the TPR profile of Ru was relatively sharp and ended at ~ 120 °C, while that of Pt was moderately sharp and ended at ~ 200 °C and that of Pd was broad and exhibited a shoulder at ~ 110 °C and another two very wide shoulders at its tail to end at ~ 300 °C. From the above discussion of H_2-TPR profiles, it can be inferred that Ru was

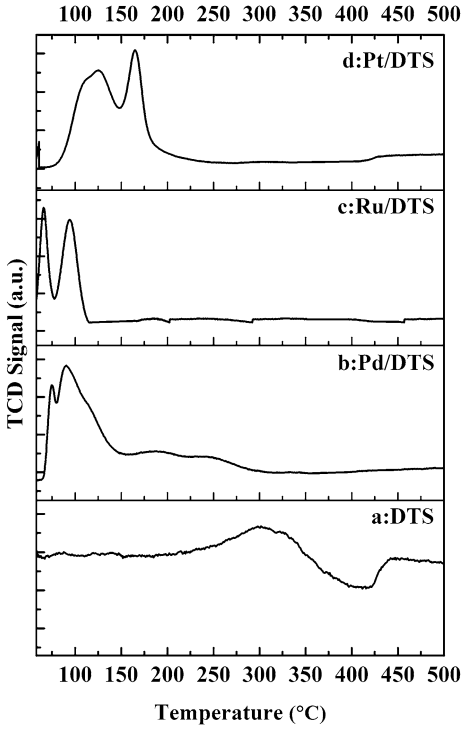

Fig. 4 H_2-TPR profile of Pd, Ru, and Pt NPs supported on DTS

Table 2 Chemisorption studies of the noble metallic surface area and dispersion obtained by using CO

Catalyst	Metallic surface of metal (m^2/g)	Metal dispersion (%)
Ru/DTS	2.49	1.1
Pd/DTS	4.79	1.9
Pt/DTS	13.2	5.37

the easiest noble metal to be reduced over DTS and had the lowest interaction with this support. On the other extreme, Pd was the most difficult noble metal to be reduced and had the strongest level of interaction with DTS support. Between the two extremes of Ru and Pd, Pt stands out in terms of exhibiting comparative reduction and interaction over DTS.

3.6 CO-Pulse Chemisorption

The CO pulse chemisorption study was conducted in order to assess the influence of the active noble metal nanoparticles on the photocatalytic activity of RhB. It is clear from Table 2 that the nature of noble metal particles has a significant impact on the metallic surface area and the metal dispersion of each photocatalyst. It was observed from Table 2 that among all of the photocatalysts, Pt/DTS displays high Pt metallic surface areas of 13.2 m^2/g and good dispersion of 5.37%. Nevertheless, Pd/DTS and Ru/DTS showed a much lower metallic surface and metal dispersion compared to Pt/DTS. Therefore, the higher photocatalytic activity of Pt/DTS than that of Pd and Ru supported on DTS could be attributed to the remarkably higher Pt metallic surface area and the metal dispersion of Pt/DTS.

3.7 Adsorption and Photocatalytic Activity Result

Prior to irradiation with UV A light, adsorption studies in the dark were primarily conducted using photocatalyst samples. The results showed that adsorption reached a steady state after 40 min, indicating the establishment of an adsorption/desorption equilibrium time between RhB in the solution and the surface of the photocatalyst. Therefore, 40 min was selected as adsorption/desorption equilibrium time and a 3.0-mL sample from the reaction mixture was then taken and labeled as time zero. The reaction mixture was then irradiated with UV A light and a 3.0-mL sample was taken at an interval of every 10 min to monitor the progress of RhB photodegradation, as shown in Fig. 5a–d.

The change in RhB concentration was calculated from the reduction of its maximum absorbance at 554 nm. As Fig. 5 illustrates, the degradation efficiency of RhB was found to decrease based on the nature of noble metal nanoparticles applied to the system. According to Fig. 5a, the absorbance peaks at 554 nm by using pure DTS decreased with increasing irradiation time, where the absorbance peak did not vanish after 80 min of UV irradiation. However, the presence of noble metal nanoparticles on the surface of DTS profoundly improved the photocatalyst activity through improving the charge separation and minimizing the recombination of excitons. This enhancement in charge separation could be attributed to the scavenging ability of noble metal of the photogenerated electrons from the interface between the noble metal nanoparticle and the DTS support [50, 51]. In case of Pd/DTS, the characteristic absorbance band of RhB at 554-nm decreased gradually with increasing irradiation time until its disappearance at 80 min, as shown in Fig. 5b. In case of Ru/DTS (Fig. 5c), the photodegradation activity was better in comparison to Pd/DTS and the RhB abated completely following a period of 50 min. The characteristic absorbance of RhB almost disappeared after 20 min when using Pt/DTS (Fig. 5d), which is the best photocatalyst among the others.

Figure 6 shows that the photocatalytic degradation of RhB over the prepared catalyst, where it again reflected the

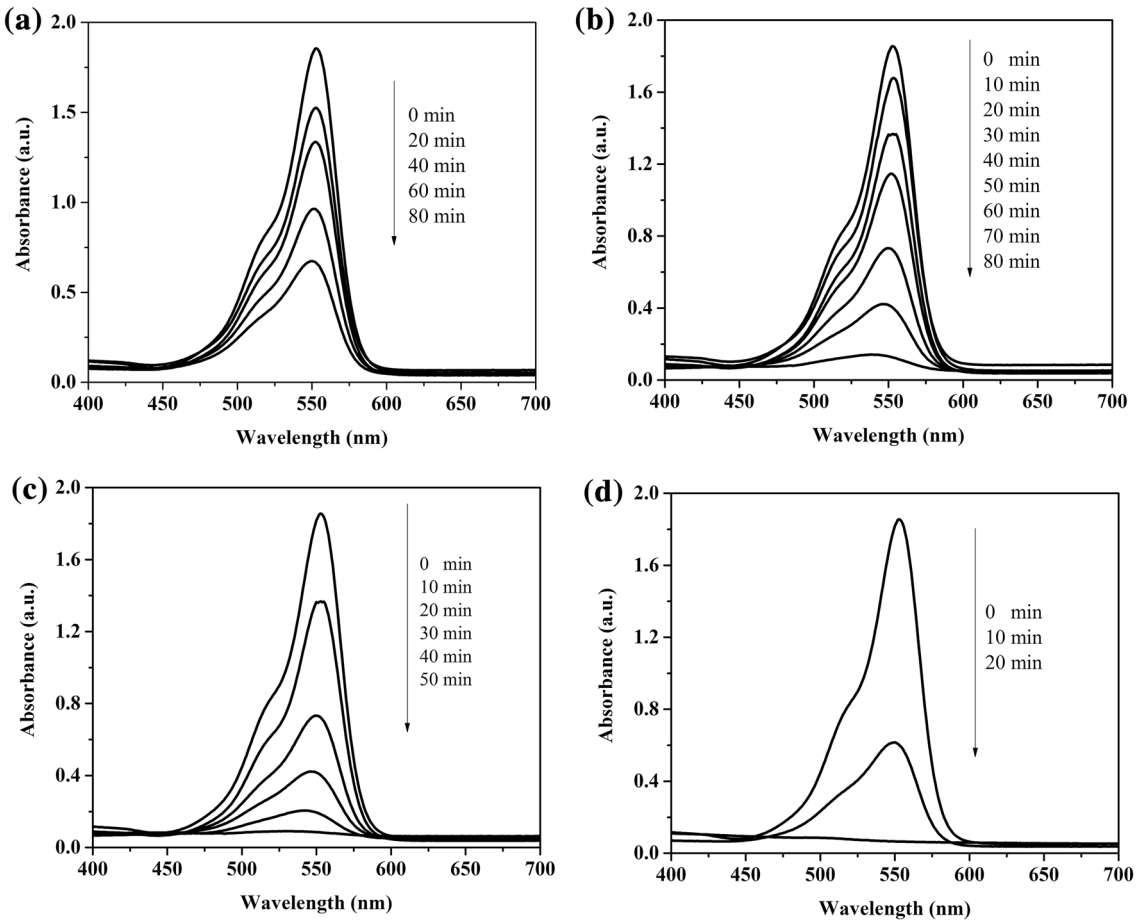

Fig. 5 Visible spectra of RhB at various reaction time, under UV irradiation, over pure DTS (**a**), Pd (**b**), Ru (**c**), and Pt (**d**) NPs supported on DTS

influence of the identity of noble metal nanoparticles on DTS photocatalytic activity. A blank test (without photocatalyst) showed that almost 97% of RbB remained after 90 min of UV irradiation. As Fig. 7 illustrates, among all of the photocatalysts, Pt/DTS showed the maximum dye adsorption (ca. ~ 7.0%) in the absence of UV irradiation. The RhB photodegradation reactions over pure DTS reached 70% after 90 min. However, loading 1.0 wt/wt% of Pd nanoparticle on DTS resulted in 98% degradation efficiency after 80 min of the reaction, while the Ru/DTS photocatalyst caused 98% degradation efficiency after 50 min. On the other hand, Pt/DTS photocatalyst showed superior photocatalytic degradation capability where almost 90% of the dye abated after 10 min with a figure of 98% after 20 min. Afterwards, the performance of Pt/DTS become stable at this value with the progress of reaction. This was probably due to the accumulation of products on the surface of the catalyst.

The kinetics of photodegradation of RhB over DTS and noble metal nanoparticles supported DTS was explored and it was found to abide with apparent first-order model, as displayed in Fig. 7. Table 3 illustrates the apparent reaction rate (k) over the tested photocatalyst, where it was found that k increased in the following order: DTS < Pd/DTS < Ru/DTS < Pt/DTS. This sequence is in agreement with the photocatalytic activity observance.

4 Conclusion

Pt, Pd and Ru nanoparticles supported on commercial DTS were successfully synthesized and their photo activity performance evaluated for the photodegradation of RhB under UV A light. The photocatalytic activity of DTS was improved by loading 1 wt/wt% of Pt, Pd and Ru metal nanoparticles. The noble metal nanoparticles functioned as a drain for electrons, which in turn, improved charge separation and minimized the recombination of excitons. In addition, photocatalytic results confirmed that PtNPs supported on DTS was the most optimal due its highest metal dispersion, highest absorbance and lowest reflectance of light

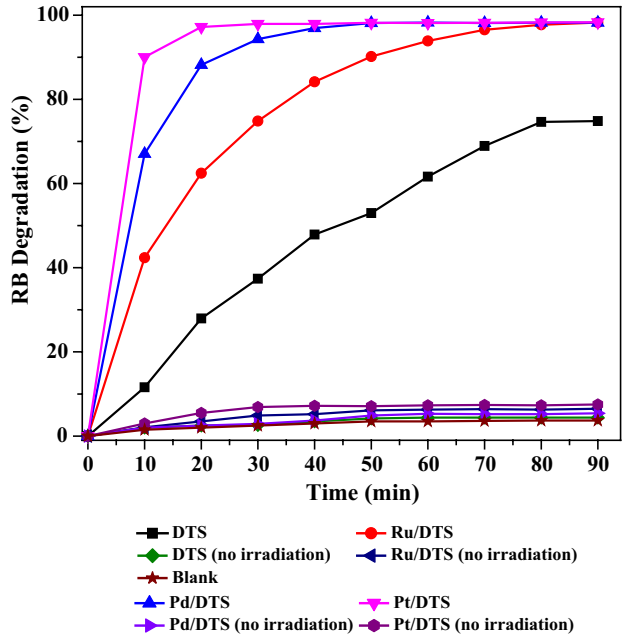

Fig. 6 Photodegradation of RhB under UV irradiation, over DTS, Pd, Ru, and Pt NPs supported on DTS

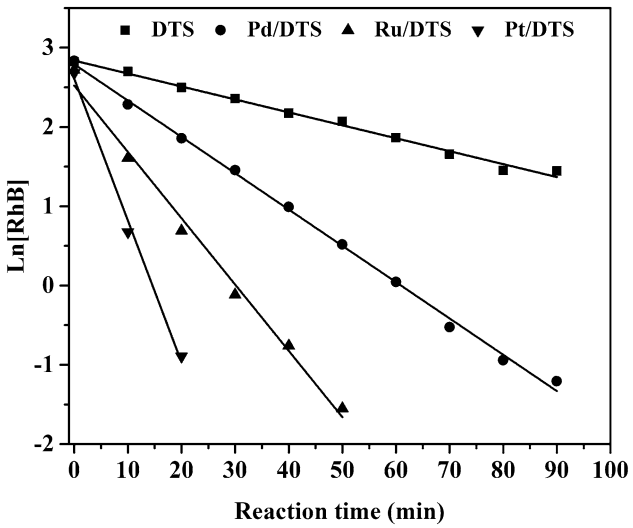

Fig. 7 First order kinetics plot for the photodegradation of RhB over DTS, Pd, Ru, and Pt NPs supported on DTS (Table 2). Apparent reaction rate for the photodegradation or RhB

Table 3 k_{app} of the pseudo first-order RhB photodegradation reaction

Photocatalyst	k_{app} (min^{-1})
DTS	0.0163
Pd/DTS	0.0458
Ru/DTS	0.0836
Pt/DTS	0.1787

as well as its smallest E_g. It was able to abate 98% of the dye after 20 min. Ru/DTS showed photocatalytic activity beneath Pt/DTS, but higher than that of Pd/DTS. The results clearly indicated that the identity of noble metal nanoparticles had a strong influence on the optical properties, which in turn, was reflected in the photocatalytic activity.

References

1. Luan JF, Li M, Ma K (2011) Chem Eng J 167:162–171
2. Singh IB, Chaturvedi KR, Morchhale KA, Yegneswaran H (2007) J Hazard Mater 141:215–222
3. Sakthivel S, Neppolian B, Shankar MV, Arabindoo B, Palanichamy M, Murugesan V (2003) Sol Energy Mater Sol Cells 77:65–82
4. Shukla SP, Gupta GS (1992) Ecotoxicol Environ Saf 24:155–163
5. Galindo C, Jacques P, Kalt A (2001) Chemosphere 45:997–1005
6. Slokar YM, Marechal AML (1998) Dyes Pigments 37:335–356
7. Gupta VK, Mohan D, Sharma S, Sharma M (2000) Sep Sci Technol 35:2097–2113
8. Bagabas A, Gondal M, Dastageer A, Yamani Z, Ashameri M (2010) Stud Surf Sci Catal 175:279–282
9. Silva CG, Sampaio MJ, Carabineiro S, Oliveira J, Baptista DL, Bacsa R, Machado BF, Serp P, Figueiredo JL, Silva A, Faria JL (2014) J Catal 316:182–190
10. Scuderi V, Impellizzeri G, Romano L, Scuderi M, Nicotra G, Bergum K, Irrera A, Svenson BG, Privitera V (2014) Nanoscale Res Lett 9:458–465
11. Kim S, Hwang SJ, Choi W (2005) J Phys Chem B 109:24260–24267
12. Li L, Yang YL, Liu XR (2013) Appl Surf Sci 265:36–40
13. Khalid NR, Ahmed E, Hong ZG, Ahmad M (2012) Appl Surf Sci 263:254–259
14. Kuang JD, Lin BZ, Chen YL, Pian XT, Zh Zhang K, Zhang O (2010) Chin J Catal 31:1399–1405
15. Xie MZ, Jing LQ, Zhou J, Lin JS, Fu HG (2010) J Hazard Mater 176:139–145
16. Brongersma ML, Halas NJ (2015) Nat Nanotechnol 10:25–34
17. Linic S, Aslam U, Boerigter C, Morabito M (2015) Nat Mater 14:567–576
18. Yin S, Zhang Q, Saito F, Sato T (2003) Chem Lett 32:358–359
19. Pelaez M, Nolan NT, Pillai SC, Seery MK, Falaras P, Kontos AG, Dunlop PSM, Hamilton JWJ, Byrne JA, O'Shea K, Entezari MH, Dionysiou DD (2012) Appl Catal B 125:331–349
20. Chatterjee D, Mahata A (2001) Appl Catal B 33:119–125
21. Han C, Likodimos V, Khan JA, Nadagouda MN, Andersen J, Falaras P, Rosales-Lombardi P, Dionysiou DD (2014) Environ Sci Pollut Res 21:11781–11793
22. Zang Y, Farnood R (2008) Appl Catal B 79:334–340
23. Sclafani A, Herrmann JM (1998) J Photochem Photobiol, A 113:181–188
24. Wold A (1993) Chem Mater 5:280–283
25. Rupa AV, Divakar D, Sivakumar T (2009) Catal Lett 132:259–267
26. Gaya UI, Abdullah AH (2008) J Photochem Photobiol, C 9:1–12
27. Makarova OV, Rajh T, Thurnauer MC (2000) Environ Sci Technol 34(4797):4803
28. Panpranot L, Kontapakdee K, Praserthdam P (2006) Appl Catal A 314:128–133
29. Maffucci L, Iengo P, Di Serio M, Santacesaria E (1997) J Catal 172:485487
30. Yang L, Liya EY, Ray MB (2008) Water Res 42:3480–3488

31. Moctezuma E, Leyva E, Aguilar CA, Luna RA, Montalvo C (2012) J Hazard Mater 243:130–138
32. Yang L, Liya EY, Ray MB (2008) Environ Sci Technol 43:460–465
33. Rachel A, Sarakha M, Subrahmanyam M, Boule P (2002) Appl Catal B 37:293–300
34. Bickley RI, Carreno TG, Lees JS, Palmisano L, Tilley RJD (1991) J Solid State Chem 92:178–190
35. Ohno T, Sarukawa K, Tokieda K, Matsumura M (2001) J Catal 203:82–86
36. Muggli DS, Ding L (2001) Appl Catal B 32:181–194
37. Saquib M, Muneer M (2003) Dyes Pigments 56:37–49
38. Qamar M, Saquib M, Muneer M (2005) Dyes Pigments 65:1–9
39. Giwa A, Nkeonye PO, Bello KA, Kolawole EG (2012) Int J Appl Sci Technol 2:90–105
40. Muruganandham M, Shobana N, Swaminathan M (2006) J Mol Catal A 246:154–161
41. Zhang Z, Wang CC, Zakaria R, Ying J (1998) J Phys Chem B 102:10871–10878
42. Yoneyama H, Yamanaka S, Haga S (1989) J Phys Chem 93:4833–4837
43. Nishimoto SI, Ohtani B, Kajiwara H, Kagiya TJ (1985) Chem Soc Faraday Trans 16:61–68
44. Zheng RB, Meng XW, Tang FQ (2009) Appl Surf Sci 255:5989–5994
45. Paola AD, Ikeda S, Marcì G, Ohtani B, Palmisano L (2002) Catal Today 75:171–176
46. Chen X, Mao SS (2007) Chem Rev 107:2891–2959
47. Das TK, Ilaiyaraja P, Mocherl PSV, Bhalerao GM, Sudakar C (2016) Sol Energy Mater Sol Cells C 144:194–209
48. Pelaez M, Nolan NT, Pillai SC, Seery MK, Falaras P, Kontos AG, Dunlop PS, Hamilton JW, Byrne JA, O'Shea K (2012) Appl Catal B 125:331–349
49. Zheng Z, Huang BB, Qin XY, Zhang XY, Dai Y, Whangbo MH (2011) J Mater Chem 21:9079–9087
50. Melvin AA, Illath K, Das T, Raja T, Bhattacharyya S, Gopinath CS (2015) Nanoscale 7:13477–13488
51. Devi LG, Kavitha R (2016) Appl Surf Sci 360:601–622

Publisher's Note Springer Nature remains neutral with regard to jurisdictional claims in published maps and institutional affiliations.